Northumbria Research Link

This version was downloaded from Northumbria Research Link: http://nrl.northumbria.ac.uk/id/eprint/27638/

Northumbria University
NEWCASTLE

UniversityLibrary

Room-temperature high performance H_2S sensor based on porous CuO nanosheets prepared by hydrothermal method

Zhijie Li[1*], Ningning Wang[1], Zhijie Lin[1], Junqiang Wang[1], Wei Liu[1], Kai Sun[2], Yong Qing Fu[1,3*], Zhiguo Wang[1*]

[1]School of Physical Electronics, University of Electronic Science and Technology of

China, Chengdu 610054, PR China

[2]Department of Nuclear Engineering and Radiological Sciences, University of Michigan,

Ann Arbor, MI 48109-2104, USA

[3]Faculty of Engineering and Environment, Northumbria University, Newcastle Upon

Tyne NE1 8ST, UK

_____

* Corresponding author. Tel.: +86 02883200728. E-mail address: zhijieli@uestc.edu.cn (Zhijie Li);
Richard.fu@northumbria.ac.uk (Yongqing Fu); zgwang@uestc.edu.cn (Zhiguo Wang).

Abstract

Porous CuO nanosheets were prepared on alumina tubes using a facile hydrothermal method, and their morphology, microstructure and gas sensing properties were investigated. The monoclinic CuO nanosheets had an average thickness of 62.5 nm and were embedded with numerous holes with diameters ranging 5 nm to 17 nm. The porous CuO nanosheets were used to fabricate gas sensors to detect hydrogen sulfide (H_2S) operated at room temperature. The sensor showed a good response sensitivity of 1.25 with the respond/recovery time of 234 s and 76 s, respectively, when tested with the H_2S concentrations as low as 10 ppb. It also showed a remarkably high selectivity to the H_2S, but only minor responses to other gases such as SO_2, NO, NO_2, H_2, CO and C_2H_5OH. The working principle of the porous CuO nanosheets based sensor to detect the H_2S was identified to be the phase transition from semiconducting CuO to a metallic conducting CuS.

1. Introduction

H₂S is one of the most common toxic contaminants, which are frequently utilized in various fields, including oil, gas, waste treatment and paper industries.[1,2] It is also commonly found or generated from sewage, rubbish dumps as well as many routine chemical production processes. Even in the presence of trace amounts, the H_2S gas is extremely toxic to many organisms, such as human respiratory and nerve system. Generally, it is recommended that the acceptable ambient levels of the H_2S for a healthy condition are in the range of 20-100 ppb.[3] Therefore, in the views of environmental protection, safety and health conditions of human being, it is urgently required to develop cheap, efficient, highly sensitive and mass-produced H_2S sensors working at room temperature, also with other advantages of excellent selectivity and reliability even as low as ppb concentration. Various H_2S gas sensors fabricated using different types of semiconductor oxides have been investigated, including In_2O_3,[4,5] ZnO,[6] SnO_2,[7] WO_3,[8] Fe_2O_3 and CuO.[9–14] Among them, CuO based nano-materials have received significant attention recently due to its excellent sensing performance.

Generally, chemical, physical, mechanical and optical properties of the nanomaterials are strongly dependent on their nanostructure and morphology. There are lots of reports recently on the synthesis of various types of the CuO nanostructures, which include nanoparticles,[15] nanoneedle,[16] nanowires,[17] nanoflowers,[18,19] nanotube,[20] nanorods,[21] nanoleaves and nanosheets.[22–29] Among these, the 2D sheet-like CuO nanostructures have received considerable attention because of their high anisotropy and nano-scale

thickness. The nano-porous structures of CuO sheets could allow a fast and efficient gas adsorption on their surfaces, thus the response times of gas sensor will be significantly decreased. However, as far as we have known, there are few reports using these CuO sheet-like nano-porous structures for gas sensing applications.

The sensing mechanism of a commonly used semiconductor gas sensor is based on the reactions of the absorbed target molecules with the metal oxide materials. For the electrical resistance based metal oxide H_2S sensors, these reactions will occur between the H_2S molecule and the oxygen ions on the surface of the metal oxides, thus generating free electrons and thus resulting in changes in the electrical resistance of the metal oxides. However, the similar reaction on the CuO materials and the associated changes in the resistance are also commonly observed in absorption of other types of reducing gases, including CO,[11,30] alcohol,[31,32] methane and ammonia gases.[33,34] Therefore, the specific H_2S sensors with a good selectivity should be explored.

In this paper, using a hydrothermal preparation process, porous CuO nanosheets were prepared on alumina tubes, on which, the resistance based H_2S gas sensors were fabricated, and their sensing performance was systematically studied.

2. Experiment

2.1 Preparation of porous CuO nanosheets

Copper chloride ($CuCl_2 \cdot H_2O$), NaOH and sodium dodecyl benzene sulfonate ($C_{18}H_{29}NaO_3S$) of analytical grades (Sinopharm Co. Ltd., China) and H_2O (with a resistivity reading of 18.0 M$\Omega \cdot$cm) were used. In a typical synthesis process, $CuCl_2 \cdot 2H_2O$ of 1.70 g were dissolved into 25 ml distilled water under a continuous stirring at room temperature to form a 0.4 M $CuCl_2 \cdot 2H_2O$ homogeneous solution. Subsequently, $C_{18}H_{29}NaO_3S$ of 3.48 g was mixed into the $CuCl_2 \cdot 2H_2O$ solution under a continuous stirring. NaOH (4 mol/L) with 15 ml volume was gradually dripped into the prepared solutions within 10 minutes to obtain a blue-colour solution. The obtained solution was placed inside a 50 ml Teflon-lined stainless autoclave, and tubes of alumina (1.5 mm of outer diameter and 4 mm long) were placed vertically on the bottom of the autoclave. The chemical reactions in the autoclave took about 24 hours with a constant temperature oven of 120 ^{o}C. After the reaction, it was naturally cooled down to room temperature (~25 ^{o}C). The alumina tubes were found to be covered with a layer of black precipitates of CuO materials. These alumina tubes were flushed with the distilled water for 3 times, and then washed with alcohol for 3 times. Finally, the alumina tubes with CuO materials were dried at 55 ^{o}C for 6 hours and annealed for 2 hours in air at 600 ^{o}C.

2.2 Characterization of CuO samples

The XRD spectrum of the porous CuO nanosheets was measured by a D/MAX2500 diffractometer with a copper target of 1.5406 Å of wavelength, operated with

voltage/current of 40 kV/30 mA. Scanning electron microscope (SEM, Inspect F50) was used to investigate the morphologies of the CuO nanosheets. The crystallographic features were also analyzed using a scanning transmission electron microscope (STEM, JEOL 3100R5) operated using a 300 kV Cold field emission gun (STEM). Surface areas of the CuO nano-sheets were characterized based on the Brunauer−Emmett−Teller (BET) method. The measurement was operated using an equipment (Tristar 3000, Micromeritics) for detecting the N_2 adsorption on the nanosheet surfaces at a temperature of 77 K. Chemical binding analysis was performed by an X-ray photoelectron spectrograph (XPS, KratosAxis-Ultra DLD), operated using a monochromatic Al Kα source with a source energy of 1486.6 eV. UV−vis spectroscopy was recorded using a UV-2101 spectrophotometer (Shimadzu Corporation, Japan).

2.3 Manufacture and testing of gas sensor

The alumina tubes coated with the porous CuO nanosheets were used to directly fabricate the sensors. The surfaces of the alumina tubes were covered with a layer of the porous CuO nanosheets layer (as shown in the schematic illustration of Figure S1 in the Supporting Information).[9] At opposite ends of the alumina tube, there was a Pt wire connected to gold electrode. The electric current of the sensor was recorded using a Keithley 2400 source meter with an applied working voltage of Vs= 0.25 V. In this paper, the definition of gas response (S) for the gas sensor is following the ideas reported in literature[9]: S=R_a/R_g, in which R_g and R_a are the resistance of CuO nanosheets layer measured in the H_2S and air, respectively.[9] All the testing gases were

commercially ones. In a standard testing process, the gas sensor was placed in a chamber of two liters and a fixed relative humidity of 30%. During the gas sensing test, the concentrations of the gas were adjusted based on the injected volumes of the H_2S.

3. Results and discussion

3.1 Structural characterization

The SEM images of the CuO samples are shown in Figure 1. Clearly, the CuO nanosheet structures can be identified, which have the average widths and lengths of about 0.5 µm and 1.2 µm, respectively. The average thickness of the CuO nanosheets is 62.5 nm. The STEM image shown in Figure 2a confirms the sheet-like CuO structures. From the STEM dark field image in Figure 2b, there are many pores with diameters ranging from 5 nm to 17 nm inside these nanosheets (see the areas with red circles). The porous structure is obviously different from the literature for those leaves-like or sheet structures of CuO.[25-39] The surface area of these CuO nanosheets obtained based on the BET method is 10.03 $m^2 \cdot g^{-1}$. These porous CuO nanosheets are efficient for the gas flowing in and out, thus enhancing their gas sensing performance. The crystalline structure in Figure 2c shows a well-defined crystal structure with lattice spacings of 0.231 and 0.196 nm, which were identified as the (200) and (20$\bar{2}$) planes of CuO, respectively.

The XRD spectrum of the porous CuO samples is shown in Figure 3, revealing the monoclinic CuO structures (JCPDS No. 48-1548). The lattice constants are a = 0.4688, b = 0.3423 and c = 0.5132 nm. No characteristic peaks from the other phases were

identified, meaning that the porous CuO nanosheets are composed of a single phase monoclinic CuO.

In the synthesis process of the porous CuO nanosheets, the ratio of Cu^{2+} and NaOH was 1:6. It was previously reported that, in the NaOH aqueous solution with a high concentration, the Cu^{2+} ions produced a square-planar complex $[Cu(OH)_4]^{2-}$ ions, rather than $Cu(OH)_2$ (as can be seen from chemical equation 1 below).[35]

$$Cu^{2+}+4OH^-\rightarrow[Cu(OH)_4]^{2-} \tag{1}$$

$$[Cu(OH)_4]^{2-}\rightarrow Cu(OH)_2\downarrow+OH^- \tag{2}$$

$$Cu(OH)_2\rightarrow CuO+H_2O \tag{3}$$

During decompositions in the hydrothermal process, because of coordination self-assembly of $[Cu(OH)_4]^{2-}$ ions, $Cu(OH)_2$ is easily formed into 2D layered orthorhombic nanostructures (see chemical equation 2).[36] Therefore, once the nuclei was formed on the surface of alumina tube, the $Cu(OH)_2$ nanosheets could start to grow. It is likely that some sodium dodecyl benzene sulfonate ligands were trapped in these nanosheets. The $Cu(OH)_2$ was then transformed into CuO structures in the post-hydrothermal process which is under high temperature and pressure (see chemical equation 3). At the same time, the trapped sodium dodecyl benzene sulfonate was released and nano-pores were formed in the CuO nanosheets.

The porous CuO nanosheets showed a broad absorption from 200 nm to 800 nm (as shown in the UV-vis absorbance spectrum of Figure S2a in the Supporting Information). The band gap energy can be obtained by the standard Tauc's relationship.[37] Based on this classical Tauc approach, the E_g value of the porous CuO nanosheets of 3.08 eV can be obtained by extrapolating the value at α=0 (as shown in

the $(\alpha h\nu)^2$ vs $h\nu$ curve of Figure S2b in the Supporting Information). This value is significantly larger than the band gap energy values of the bulk CuO crystals of 1.85 eV.[37] The larger E_g values of various CuO nanostructures have been reported, such as 3.48 eV for ultra-long CuO nanowires,[38] 3.55 eV for CuO nanoplates,[39] and 3.02 eV for CuO nanoplatelets.[40] It has been reported that the specific sites of molecular adsorption were remarkably influenced by the band gap energy, and thus could remarkably influence the gas sensitive property.[37,38]

3.2 Sensing performance

Figure 4 shows the response/recovery curves of the gas sensor based on CuO nanosheets to H_2S from 10 ppb to 60 ppm at room temperature. The porous CuO nanosheets sensor provides a stable baseline in the dry air condition before the sensing measurement at different concentrations. Upon the H_2S injection, a positive sensor response was obtained, meaning that resistance was decreased drastically. After the H_2S gas was pumped away, the signal was returned back to its initial stable baseline. The sensitivity values of the porous CuO nanosheets sensor to various concentrations of the H_2S were calculated, and the results are shown in Figure 5a. The inset of Figure 5a shows the sensitivity values to sub-ppm concentrations of H_2S. The sensitivity of the sensor increases with the increasing concentrations of the H_2S. Even with the H_2S concentration as low as 10 ppb, the sensor still has good response sensitivity value about 1.25 at room temperature as shown in Figure 4a and Figure 5a.

Most previously published papers reported that the H_2S sensing could be successfully performed at a relatively high temperature. For example, Steinhauer et

al[11] reported the detection of 10 ppb H_2S using a CuO nanowire based sensor at 325 $^{\circ}C$, and Zhang et al[14] reported the detection of 30 ppb H_2S using CuO nanosheet based sensor at 240 $^{\circ}C$. Although Ramgir et al reported a room temperature operated sensor using CuO thin films, the detection limit to H_2S was higher than 100 ppb.[12] Therefore, we can confirm that at room temperature, our sensor based on the porous CuO nanosheets in this study has an excellent property for detecting hydrogen sulfide at lower concentrations.

Figure 5b shows the response/recovery times of the porous CuO nanosheets based sensor. The definition of response/recovery times was based on the report of the literature.[9] There was an obvious change of the response/recovery times based on the results shown in Figure 5b. The response times were in the range from 41 s to 606 s when the H_2S concentrations were changed from 10 ppb to 60 ppm. However, when the H_2S gas concentration was higher than 1 ppm, it was less than 90 s. The recovery time is in the range from 17 s to 1173 s, but it was less than 76 s when the concentration of H_2S was less than 0.04 ppm. It can be concluded that the huge amount of nanopores in the nanosheets (as shown in Figure 2b) are favorite for both absorption/desorption of H_2S gas, leading to the shorter response/recovery times.

Besides the high sensitivity, the reproducibility of the gas sensor is another important performance indicator. Figure 6a shows the reproducibility testing results of the porous CuO nanosheets based sensor, which was successively exposed to 200 ppb H_2S for five times at the room temperature. Clearly a good reproducibility was obtained. During the repeated absorption/desorption of the H_2S, the dynamic curves

for five times are almost identical. It shows a stable response curve with a maximum response sensitivity about 5.01 to 200 ppb H_2S.

Long-term stability is also a critical parameter for the application of gas sensor. The measurement readings of the porous CuO nanosheets based H_2S sensor were recorded for a month, and the result are plotted in Figure 6b. The response deviation when the device was exposed in 200 ppb H_2S is lower than 5% after long-term testing for a month, indicating that the CuO nanosheet sensor has a good long-term stability.

The selectivity of a gas sensor is another critical parameter. Figure 7 shows the response curves of the sensor exposed to various gases (SO_2, NO, NO_2, H_2, CO, C_2H_5OH and NH_3) at the same gas concentration of 40 ppm compared with the H_2S of 0.2 ppm at room temperature. It is obvious that, compared with the remarkable responses to the 0.2 ppm H_2S, there was no responses of the gas sensor to 40 ppm SO_2, NO, NO_2, CO, H_2 and C_2H_5OH. Only one exception is the 40 ppm of NH_3, with a low response sensitivity of 1.42. However, it is clear that the response sensitivity of 0.2 ppm H_2S was 3.5 times higher than that to the 40 ppm NH_3. The results indicated that there is a good selectivity of the porous CuO nanosheets H_2S sensor compared with the previously reported results.[11,33,41]

3.3 Gas-sensing mechanism

CuO is a p-type semiconductor, and the charge carriers are positive holes. The adsorption and desorption of the H_2S on the surface of the CuO will result in the changes of electrical resistance. According to the mechanism of oxidation of H_2S by the adsorbed oxygen ions, the resistance of the CuO will be increased.[42,43] However,

from the real-time response shown in Figure 8, it is worth mentioning that the resistance of the sensor decreased quickly upon the H_2S injection,, which is opposite to the commonly accepted mechanisms for the p-type semiconductor gas sensors. It is apparent that there is a totally different sensing mechanism of the porous CuO nanosheets with the H_2S. In this paper, we proposed that the working principle of sensor should be the transformation from CuO to CuS, the latter of which has a good metallic-like conductivity.

When the H_2S molecules are absorbed on the CuO surface, it will react with the CuO directly, based the chemical reaction 4 as shown below:[43]

$$H_2S(g) +CuO(s) \rightarrow CuS(s) +H_2O(g) \tag{4}$$
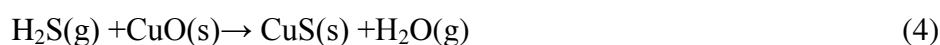
Firstly, the Cu_xS (x<1) layer is formed on the CuO surface, and then it converts to CuS layer, which covers the surface of CuO sheets. The S^{2-} ions continue to percolate inside the bulk CuO and form Cu_xS percolation regime in the sub-layer, as shown in Figure 9a. Formation of the CuS on the CuO has been proven by the XPS analysis results.[43,44] CuS, a metallic-like conductor, will increase the connectivity between the neighboring CuO sheets, leading to a decrease of the resistance of the CuO nanosheets film. The porous CuO nanosheets are convenient for the adsorption of the H_2S gas molecules, thus facilitating the transformation of CuS. Because of existence of the porous structures of the sheet-like CuO nanostructures, the reaction of CuS formation is very fast. It was 336 s to achieve a reaction equilibrium for the 200 ppb H_2S gas at room temperature as shown in Figure 8.

After the H_2S gas was replaced with the dry air, recovery of the measured response

was initiated immediately. Based on a schematic illustration of the recovery pathway as shown in Figure 9b, the CuS will transform back into CuO in air based on the chemical reaction 5 as shown below:[43]

$$2CuS(s) + 3O_2(g) \rightarrow 2CuO(s) + 2SO_2(g) \qquad\qquad (5)$$
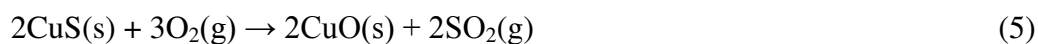
The porous structures of the CuO nanosheets are convenient for the molecular diffusion/desorpton. Therefore, the reading of the sensor can be quickly recovered at room temperature as shown in Figure 8, revealing its reliability to the applications.

XPS results confirmed the formation of CuS. Because it is quite difficult to characterize the H_2S sensing process using XPS, here, the XPS analysis was only used to prove that the CuS has formed on the surface of CuO powder. The testing sample used in the XPS analysis was CuO powder. The CuO powder was firstly placed in a chamber with the H_2S gas at room temperature, then it was taken out and measured using XPS. The CuO powder without exposed to the H_2S gas was also characterized using the XPS for a comparison. Before and after exposure in H_2S gas, the XPS spectra of Cu $2p_{3/2}$ and S 2p of the CuO nanosheets are shown in Figure 10, respectively. Before exposure in H_2S gas, the Cu $2p_{3/2}$ spectrum shows a main peak at 933.9 eV along with its satellite peaks, which are all attributed to those of the CuO.[18,45] However, for the CuO sample which had been exposed in H_2S gas, the main peak of the Cu $2p_{3/2}$ shows a broad asymmetric curve which was deconvoluted into two peaks at 932.6 and 930.8 eV, attributing to CuO and CuS, respectively.[45,46] For the S 2p spectra, the peaks at 162.3 and 163.4 eV could be identified (Figure 10b) after exposure to H_2S, which are attributed to S $2p_{3/2}$ and S $2p_{1/2}$ states respectively.

This result clearly confirms the formation of CuS.[46,47] When it was exposed to air again, the XPS spectra were found to be almost the same as those before exposure to the H_2S, indicating the transformation from the CuS to CuO.

As shown in Figure 7, when the sensor was exposed into ammonia, the resistance of the sensor was also reduced, although compared with the results from the H_2S, its response sensitivity is quite low. The sensing mechanism to the NH_3 for the CuO sensor could be explained based on proton conductivity of NH_4^+.[48] The H_2O molecules were absorbed on porous CuO nanostructures at room temperature. The absorbed NH_3 molecules could react with the H_2O molecules, based on the following chemical reaction:

$$NH_3(abs) + H_2O(abs) \leftrightarrow NH_4^+ + OH^- \tag{6}$$

Therefore, the resistance of gas sensor was decreased due to the proton conductivity of NH_4^+.[48]

4. Conclusions

In this paper, we presented the fabrication and characterization of porous CuO nanosheets on the alumina tubes. And the fabricated H_2S sensor showed an excellent sensing performance. The CuO nanosheets had an average thickness of 62.5 nm. Detailed structural analysis confirmed that the synthesized CuO nanosheets had monoclinic CuO structures, and there were many holes with a diameter ranging from 5nm to 17 nm inside the nanosheets. The working principle of sensor was attributed to the transformation of semiconducting p-type CuO to metallic CuS. The porous CuO nanosheets based H_2S sensor showed excellent gas sensitive performance and

remarkably good selectivity, which showed little responses to SO_2, NO, NO_2, H_2, CO and C_2H_5OH at room temperature, and a relatively weak response to NH_3. Therefore, the porous CuO nanosheets based sensor prepared in this study can be efficiently used for high-performance H_2S gas sensor.

ASSOCIATED CONTENT

Supporting Information available:

Measurement schematic illustration of gas sensor based on the porous CuO nanosheets sensing material.

UV–vis absorptions spectrum and (b) the corresponding plots of $(\alpha h v)^2$ vs hv curve of the porous CuO nanosheets.

AUTHOR INFORMATION

Corresponding Author

*E-mail: zgwang@uestc.edu.cn (Zhiguo Wang);

Richard.fu@northumbria.ac.uk (Yongqing Fu);

zhijieli@uestc.edu.cn (Zhijie Li);

Notes

The authors declare no competing financial interest.

References

(1) Hauppauge, *Science and Technology of Chemo Resistive Gas Sensors*; Nova Science Publisher: New York, **2007**.

(2) Mortezaali, A.; and Moradi, R. The Correlation between the Substrate Temperature and Morphological ZnO Nanostructures for H_2S Gas Sensors. *Sens. Actuators, A* **2014**, 206, 30.

(3) Kaur , M.; Jain, N.; Sharma, K.; Bhattachary, S.; Roy, M.; Tyagi, A. K.; Gupta, S. K. and Yakhmi, J. V. Room-Temperature H_2S Gas Sensing at ppb Level by Single Crystal In_2O_3 Whiskers. Sens. *Actuators, B* **2008**, 133, 456–461.

(4) Yao, K.; Caruntu, D.; Zeng, Z. M.; Chen, J. J.; O'Connor, C. J.; Zhou, W. L. Parts per Billion-Level H_2S Detection at Room Temperature Based on Self-Assembled In_2O_3 Nanoparticles. *J. Phys. Chem. C* **2009**, 113, 14812–14817.

(5) Zhang, S. C.; Huang, Y. W.; Kuang, Z.; Wang, S. Y.; Song, W. L.; Ao, D. Y.; Liu, W. and Li, Z. J. Solvothermal Synthesized In_2O_3 Nanoparticles for ppb Level H_2S Detection. *Nanosci. Nanotechnol. Lett.* **2015**, 7, 455–461.

(6) Kim, J.; Yong, K. Mechanism Study of ZnO Nanorod-Bundle Sensors for H_2S Gas Sensing. *J. Phys. Chem. C* **2011**, 115, 7218–7224.

(7) Zhang, S. M.; Zhang, P. P.; Wang, Y.; Ma, Y. Y.; Zhong, J.; Sun, X. H.; Facile Fabrication of Well-Ordered Porous Cu-Doped SnO_2 Thin Film for H_2S Sensing. *ACS Appl. Mater. Interfaces.* **2014**, 6, 14975−14980.

(8) Shen, Y. B.; Zhang, B. Q.; Cao, X. M.; Wei , D. Z.; Ma, J. W.; Jia, L. J.; Gao, S. L.; Cui, B. Y.; Jin, Y. C. Microstructure and Enhanced H_2S Sensing Properties of

Pt-Loaded WO$_3$ Thin Films. *Sens. Actuators, B* **2014**, 193, 273–279.

(9) Huang, Y.W.; Chen, W. M.; Zhang, S.C.; Kuang, Z.; Ao, D.Y.; Alkurdc, N. R.; Zhou, W. L.; Liu, W.; Shen, W.Z.; Li, Z.J. A High Performance Hydrogen Sulfide Gas Sensor Based on Porous α-Fe$_2$O$_3$ Operates at Room-Temperature. *Appl. Surf. Sci.* **2015**, 351, 1025–1033.

(10) Li, Z.J.; Huang, Y.W.; Zhang, S.C.; Chen, W.M; Kuang, Z.; Ao, D.Y.; Liu, W.; Fu, Y.Q. A Fast Response & Recovery H$_2$S Gas Sensor Based on α-Fe$_2$O$_3$ Nanoparticles with ppb Level Detection Limit, *J. Hazard. Mater.* **2015**, 300, 167–174.

(11) Steinhauer, S.; Brunet, E.; Maier, T.; Mutinati, G. C.; Köck, A.; Freudenberg, O.; Gspan, C.; Grogger, W.; Neuholde, A.; Resele, R. Gas sensing properties of novel CuO nanowire devices. Sens. Actuators, B 2013, 187, 50–57.

(12) Choi, S.W.; Katoch, A.; Zhang, J.; Kim, S. S. Electrospun Nanofibers of CuO–SnO2 Nanocomposite as Semiconductor Gas Sensors for H2S Detection, *Sens. Actuators, B* **2013**, 176, 585– 591.

(13) Li, X. P.; Wang, Y.; Lei, Y. and Gu, Z. Y. Highly Sensitive H$_2$S Sensor Based on Template Synthesized CuO Nanowires. *RSC Adv.* **2012**, 2, 2302–2307.

(14) Zhang, F.; Zhu, A.W.; Luo, Y. P.; Tian, Y.; Yang, J. H.; Qin, Y. CuO Nanosheets for Sensitive and Selective Determination of H$_2$S with High Recovery Ability. *J. Phys. Chem. C.* **2010**, 114, 19214–19219.

(15) Yin, M.; Wu, C. K.; Lou, Y. B.; Burda, C.; Koberstein, J. T.; Zhu, Y. M. and O'Brien, S. Copper Oxide Nanocrystals. *J. Am. Chem. Soc.* **2005**, 127, 9506–9511.

(16) Liu, Y. L.; Liao, L.; Li, J. C. and Pan, C. X. From Copper Nanocrystalline to CuO

Nanoneedle Array: Synthesis, Growth Mechanism, and Properties. *J. Phys. Chem. C* **2007**, 111, 5050–5056.

(17) Jiang, X. C.; Herricks, T. and Xia, Y. CuO Nanowires can be Synthesized by Heating Copper Substrates in Air. *Nano Lett.* **2002**, 2, 1333–1338.

(18) Gao, D. Q.; Yang, G. J.; Li, J. Y.; Zhang, J.; Zhang, J. L. and Xue, D. S. Room-Temperature Ferromagnetism of Flowerlike CuO Nanostructures. *J. Phys. Chem. C* **2010**, 114, 18347–18351.

(19) Li, K.; Fan, G. L.; Yang, L.; Li, F. Novel Ultrasensitive Non-enzymatic Glucose Sensors Based Oncontrolled Flower-Like CuO Hierarchical Films. *Sens. Actuators, B* **2014**, 199, 175–182.

(20) Chun, S. R.; Sasangka, W. A.; Ng, M. Z.; Liu, Q.; Du, A. Y.; Zhu, J.; Ng, C. M.; Liu, Z. Q.; Chiam, S. Y.; Gan, C. L. Joining Copper Oxide Nanotube Arrays Driven by the Nanoscale Kirkendall Effect. *Small* **2013**, 9, 2546–2552.

(21) Shrestha, K. M.; Sorensen, C. M.; Klabunde, K. J. Synthesis of CuO Nanorods, Reduction of CuO into Cu Nanorods, and Diffuse Reflectance Measurements of CuO and Cu Nanomaterials in the Near Infrared Region. *J. Phys. Chem. C* **2010**, 114, 14368–14376.

(22) Kim, H.; Jin, C.; Park, S.; Kim, S.; Lee, C. H2S Gas Sensing Properties of Bare and Pd-Functionalized CuO Nanorods, *Sens. Actuators, B* **2012**, 161, 594–599.

(23) Cao, Y.; Liu, S.Y.; Jian, X.; Zhu, G. L.; Yin, L. J.; Zhang, L.; Wu, B.; Wei, Y. F.; Chen, T.; Gao, Y. Q.; Tang, H.; Wang, C.; He, W. D. and Zhang, W. L. Synthesis of High-Purity CuO Nanoleaves and Analysis of their Ethanol Gas Sensing Properties.

RSC Adv. **2015**, 5, 34788–34794.

(24) Zhao, Y.; Zhao, J. Z.; Li, Y. L.; Ma, D. C.; Hou, S. N.; Li, L. Z.; Hao, X. L.; Wang, Z. C. Room Temperature Synthesis of 2D CuO Nanoleaves in Aqueous Solution. *Nanotechnology* **2011**, 22, 115604.

(25) Huang, J. C.; Wu, H. B.; Cao, D. X.; Wang, G. L. Influence of Ag Doped CuO Nanosheet Arrays on Electrochemical Behaviors for Supercapacitors. *Electrochim. Acta* **2012**, 75, 208–212.

(26) Zhao, J. G.; Liu, S. J.; Yang, S. H.; Yang, S. G. Hydrothermal Synthesis and Ferromagnetism of CuO Nanosheets. *Appl. Surf. Sci.* **2011**, 257, 9678–9681.

(27) Auxilia, F. M.; Ishihara, S.; Mandal, S.; Tanabe, T.; Saravanan, G.; Ramesh, G. V.; Umezawa, N.; Hara, T.; Xu, Y.; Hishita, S.; Yamauchi, Y.; Dakshanamoorthy, A.; Hill, J. P.; Ariga, K. and Abe, H. Low-Temperature Remediation of NO Catalyzed by Interleaved CuO Nanoplates. *Adv. Mater.* **2014**, 26, 4481–4485.

(28) Ibupoto, Z. H.; Khun, K.; Beni, V.; Liu, X. and Willander, M. Synthesis of Novel CuO Nanosheets and Their Non-Enzymatic Glucose Sensing Applications. *Sensors* **2013**, 13, 7926–7938.

(29) Uthirakumar, P.; Muthulingam, S.; Khan, R.; Yun, J. H.; Cho, H. S.; Lee, I. H. Surfactant-Free Synthesis of Leaf-Like Hierarchical CuO Nanosheets as a UV Light Filter. *Mater. Lett.* **2015**, 156, 191–194.

(30) Volanti, D. P.; Felix, A. A.; Orlandi, M. O.; Whitfield, G.; Yang, D. J.; Longo, E.; Tuller, H. L. and Varela, J. A. The Role of Hierarchical Morphologies in The Superior Gas Sensing Performance of CuO-Based Chemiresistors. *Adv. Funct. Mater.* **2013**, 23,

1759–1766.

(31) Zhang, J.; Liu, J.; Peng, Q.; Wang, X. and Li, Y. Nearly Monodisperse Cu_2O and CuO Nanospheres: Preparation and Applications for Sensitive Gas Sensors. *Chem. Mater.* **2006**, 18, 867–871.

(32) Yang, C.; Su, X.; Xiao, F.; Jian, J.; Wang, J. Gas Sensing Properties of CuO Nnanorods Synthesized by a Microwave-Assisted Hydrothermal Method. *Sens. Actuators, B* **2011**, 158, 299–303.

(33) Zappa, D.; Comini, E.; Zamani, R.; Arbio, J.; Morante, J. R.; Sberveglieri, G. Preparation of Copper Oxide Nanowire-Based Conductometric Chemical Sensors. *Sens. Actuators, B* **2013**, 182, 7–15.

(34) Shao, F.; Hernández-Ramírez, F.; Prades, J. D.; Fabrega, C.; Andreu, T.; Morante, J. R. Copper (II) Oxide Nanowires for P-type Conductometric NH_3 Sensing. *Appl. Surf. Sci.* **2014**, 311, 177–181.

(35) Ni, Y. H.; Li, H.; Jin, L. and Hong, J. M. Synthesis of 1D $Cu(OH)_2$ Nanowires and Transition to 3D CuO Microstructures under Ultrasonic Irradiation, and their Electrochemical Property. *Cryst. Growth Des.* **2009**, 9, 3868–3873.

(36) Wen, X. G.; Zhang, W. X. and Yang, S. H. Solution Phase Synthesis of $Cu(OH)_2$ Nanoribbons by Coordination Self-Assembly using Cu_2S Nanowires as Precursors. *Nano Lett.* **2002**, 2, 1397–1401.

(37) Santra, K.; Sarkar, C. K.; Mukherjee, M. K.; Ghosh, B. Copper Oxide Thin Films Grown by Plasma Evaporation Method. *Thin Solid Films* **1992**, 213, 226–229.

(38) Wang, W. Z.; Wang, L. J.; Shi, H. L.; Liang, Y. J. A Room Temperature Chemical

Route for Large Scale Synthesis of Sub-5 nm Ultralong CuO Nanowires with Strong Size Effect and Enhanced Photocatalytic Activity. *Cryst. Eng. Comm.* **2012**, 14, 5914–5922.

(39) Chand, P.; Gaur, A.; Kumar, A.; Gaur, U. K. Effect of NaOH Molar Concentration on Morphology, Optical and Ferroelectric Properties of Hydrothermally Grown CuO Nanoplates. *Mat. Sci. Semicon. Proc.* **2015**, 38, 72–80.

(40) Zou, G. F.; Li, H.; Zhang, D. W.; Xiong, K.; Dong, C. and Qian, Y. T.; Well-Aligned Arrays of CuO Nanoplatelets. *J. Phys. Chem. B* **2006**, 110, 1632–1637.

(41) Fu, T. CuS-Doped CuO Nanoparticles Sensor for Detection of H_2S and NH_3 at Room Temperature. *Electrochim. Acta* **2013**, 112, 230–235.

(42) Barsan, C.; Simion, T.; Heine, S.; Pokhrel, U. W. Modeling of Sensing and Transduction for P-type Semiconducting Metal Oxide Based Gas Sensors. *J. Electroceram.* **2010**, 25, 11–19.

(43) Hennemann, J.; Kohl, C.D.; Smarsly, B.M.; Metelmann, H.; Rohnke, M.; Janek, J.; Reppin, D.; Meyer, B.K.; Russ, S.; Wagner, T. Copper Oxide Based H_2S Dosimeters − Modeling of Percolation and Diffusion Processes, *Sens. Actuators, B* **2015**, 217, 41–50.

(44) Ramgir, N.S.; Ganapathi, S.K.; Kaur, M.; Datta, N.; Muthe, K.P.; Aswal, D.K.; Gupta, S.K.; Yakhmi, J.V. Sub-ppm H_2S Sensing at Room Temperature using CuO Thin Films, *Sens. Actuators, B* **2010**, 151, 90–96.

(45) Zarate, R.A.; Hevia, F.; Fuentes, S.; Fuenzalida, V.M.; Zuniga, A. Novel Route to Synthesize CuO Nanoplatelets, *J. Solid State Chem.* **2007**, 180, 1464‒1469.

(46) Liu, P.; Huang, Y.; Yan, J.; Yang, Y.W.; Zhao, Y. Construction of CuS Nanoflakes Vertically Aligned on Magnetically Decorated Graphene and Their Enhanced Microwave Absorption Properties, *ACS Appl. Mater. Interfaces.* **2016**, 8, 5536−5546.

(47) Amare, A.D.; Andebet, G.T.; Chen, H.M.; Taame, A.B.; Pan, C.J.; Su, W.N.; Hwang, B.J. A Highly Stable CuS and CuS–Pt Modified Cu_2O/CuO Heterostructure as an Efficient Photocathode for the Hydrogen Evolution Reaction, *J. Mater. Chem. A* **2016**, 4, 2205–2216.

(48) Tang, Y.L.; Li, Z.J.; Zu, X.T.; Ma, J.Y.; Wang, L.; Yang, J.; Du, B.; Yu, Q.K. Room-Temperature NH_3 Gas Sensors Based on Ag-Doped $\alpha\text{-}Fe_2O_3/SiO_2$ Composite Films with Sub-ppm Detection Ability, *J. Hazard. Mater.* **2015**, 298, 154–161.

The Table of Contents (TOC) Graphic
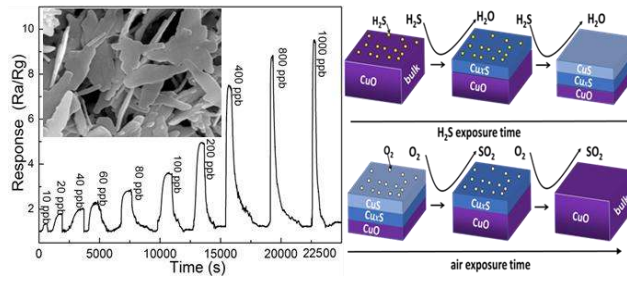
Figures
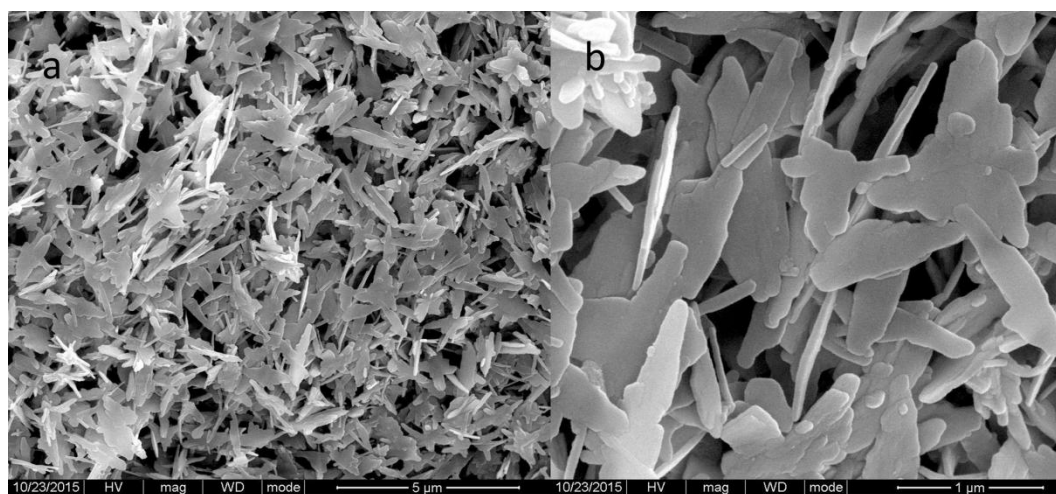
Figure 1. SEM images with different magnifications of the CuO sample (a) Low magnification; (b) High magnification.
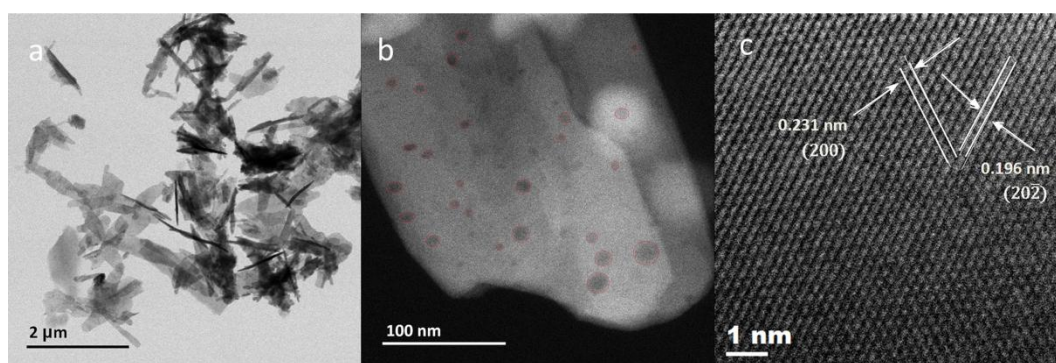
Figure 2. (a) STEM image of low magnification bright field; (b) STEM image of dark field image; (c) the crystalline framework of the CuO samples.
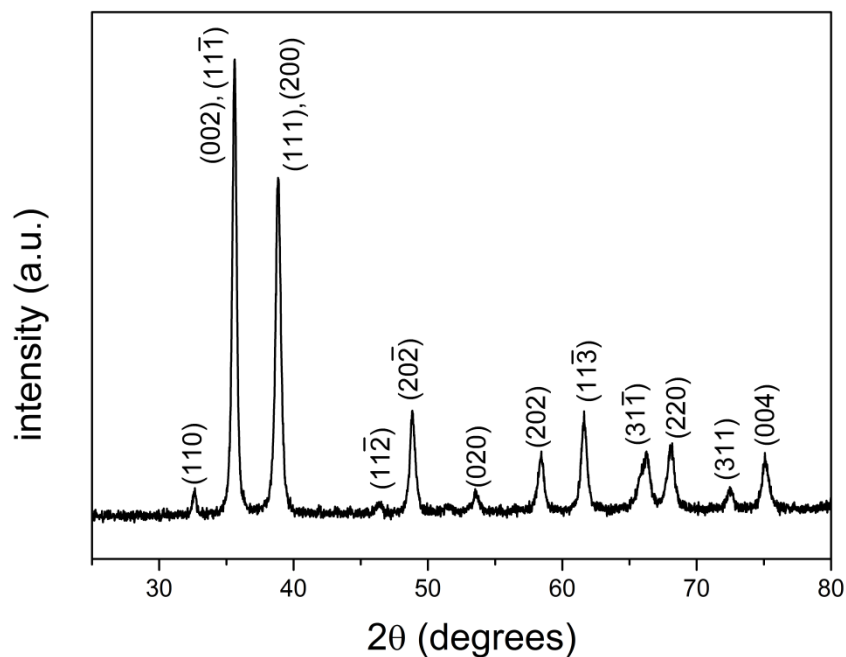
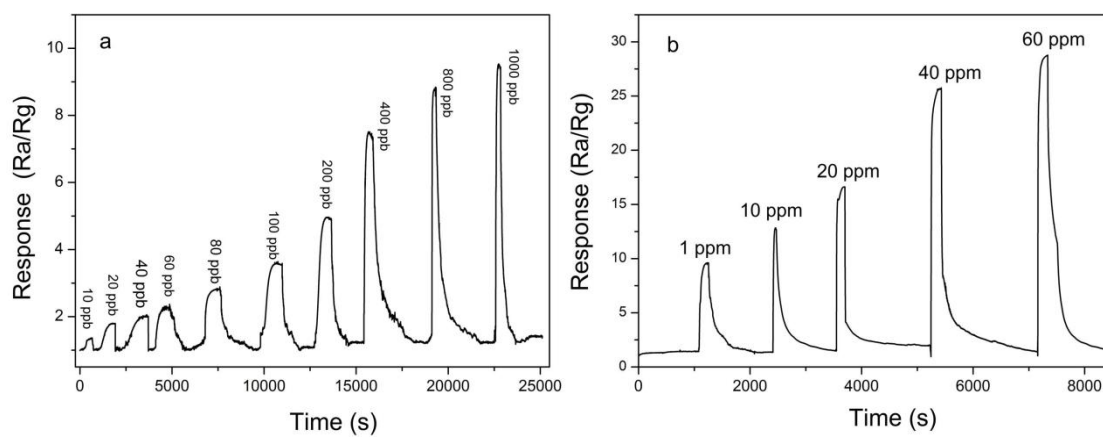Figure 3. XRD pattern of the porous CuO nanosheets.

Figure 4. Response and recovery curves of the porous CuO nanosheets based gas sensor to H$_2$S with the concentration (a) from10 ppb to 1 ppm and (b) from 1 ppm to 60 ppm at room temperature.
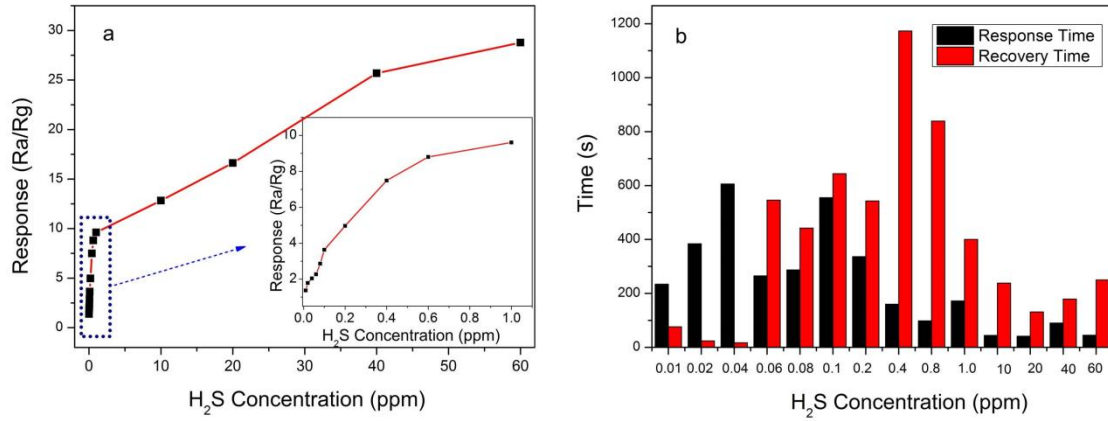
Figure 5. (a) Variation of the sensitivity and (b) Response time and recovery time of the porous CuO nanosheets based gas sensor at different H_2S gas concentration from 10 ppb to 60 ppm.
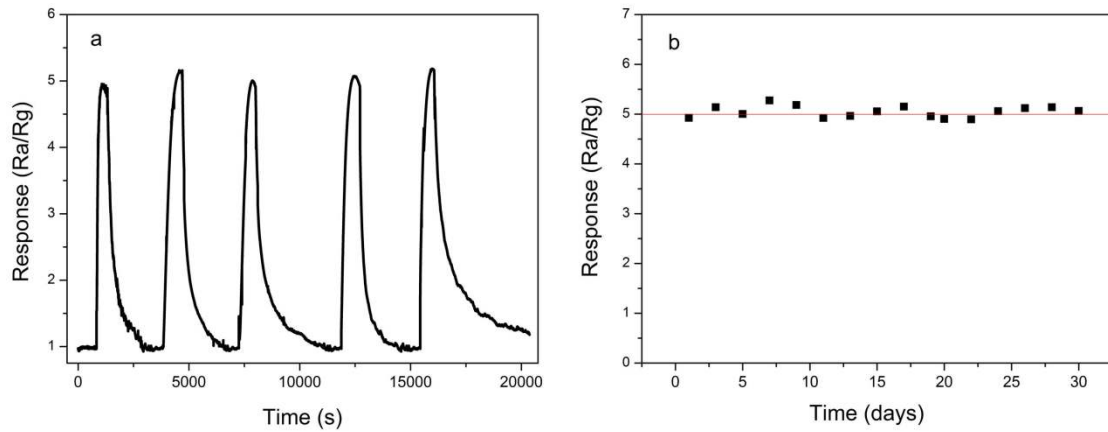
Figure 6. (a) Reproducibility and (b) Long-term stability of the porous CuO nanosheets based gas sensor exposed to 200 ppb H_2S gas for five times.
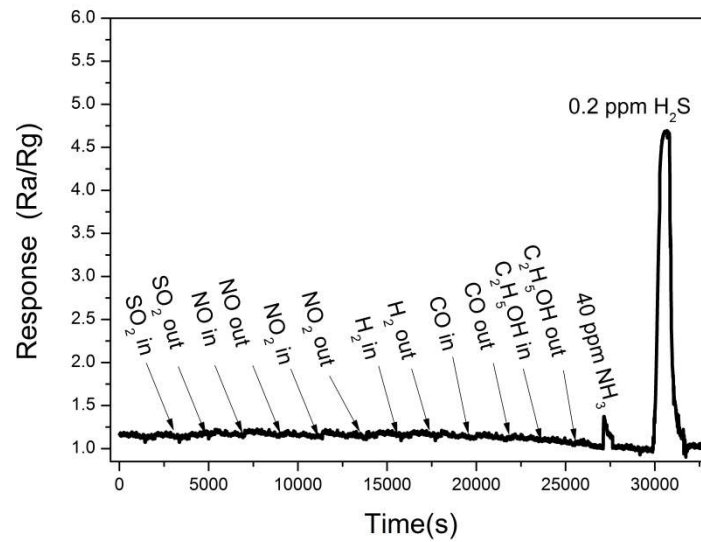
Figure 7. Response and recovery curves of the porous CuO nanosheets based gas sensors to difference gases (SO$_2$, NO, NO$_2$, H$_2$, CO, C$_2$H$_5$OH, NH$_3$) of 40 ppm and 0.2 ppm H$_2$S at room temperature.
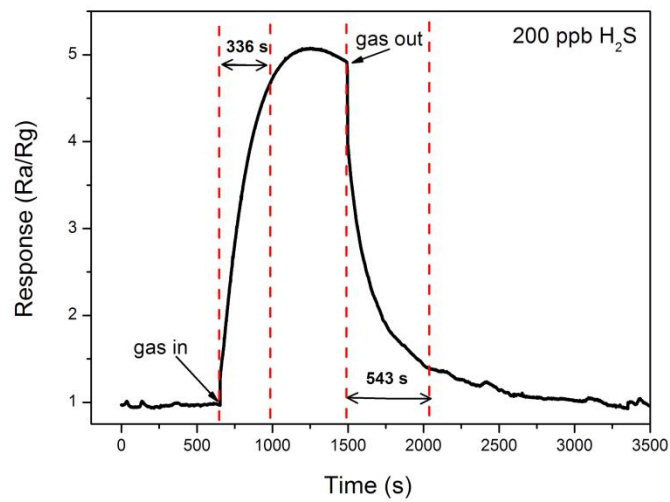

Figure 8. Real-time gas sensing curve of the sensor based on the porous CuO nanosheets to 200 ppb H$_2$S gas.
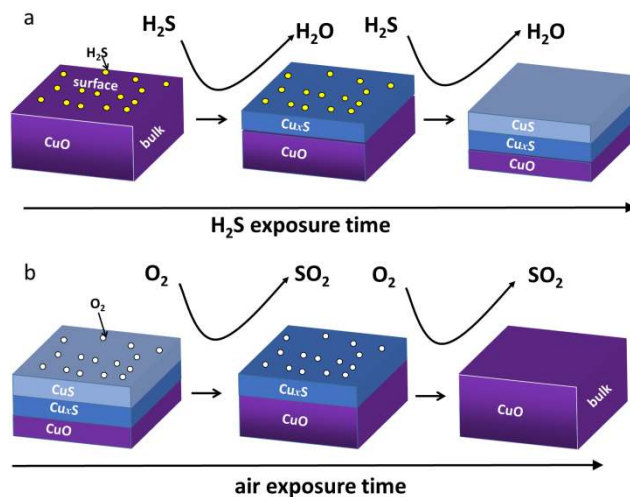
Figure 9. Schematic illustration of (a) reaction pathway in H_2S and (b) recovery pathway in air of CuO nanosheet.
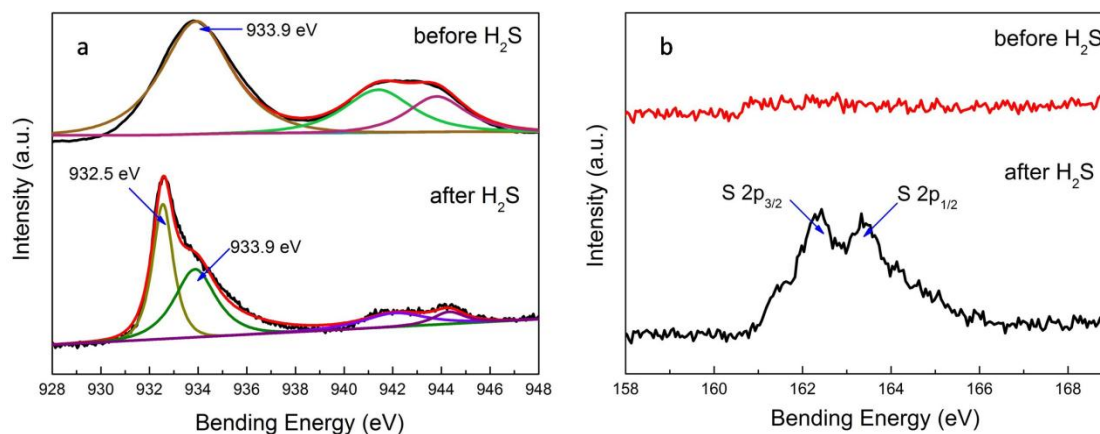

Figure 10. (a) Cu $2p_{3/2}$ and (b) S 2p XPS spectra of the CuO samples before and after exposure to H_2S.